CrossMark

In-situ polymerization growth of polyaniline nanowire arrays on graphene foam for high specific capacitance supercapacitor electrode

Xin Gao[1] · Hongyan Yue[1] · Erjun Guo[1] · Longhui Yao[1] · Xuanyu Lin[1] · Bao Wang[1] ·
Enhao Guan[1] · Dzmitry Bychanok[2]

Abstract Graphene foam (GF) was fabricated by chemical vapor deposition using nickel foam as the template and the GF was activated by concentrated nitric acid. Polyaniline nanowire arrays (PANI NWAs) were grown on the surface of GF by in-situ polymerization to obtain the PANI NWAs/ GF composite. The morphologies and structures of GF and PANI NWAs/GF composite were characterized by scanning electron microscopy, transmission electron microscopy and Raman analysis, respectively. The integration between GF and PANI NWAs shows a synergistic effect. GF provides electrically conductive channels for the PANI NWAs anchored on it, and PANI NWAs with small diameters provide high pseudocapacitance and enhanced electrode specific surface area. The electrode exhibits a high specific capacitance 870 F g^{-1} at 1 A g^{-1}. Moreover, the electrodes possess an excellent cycle life with 80% capacitance retention after 1000 cycles at 6 A g^{-1}.

1 Introduction

Supercapacitor has attracted great attention owing to their high power density, long cycling stability and fast charge–discharge rate [1–3]. Graphene is a single layer of sp^2 hybridized carbon atoms packed densely in a honeycomb lattice, which has been used as a supercapacitor electrode material due to its excellent electrical properties, ultrahigh chemical stability and specific surface area up to 2630 m^2 g^{-1} [4–6]. Although graphene is very stable as a supercapacitor electrode material, the capacitance is relatively low due to the mechanism of electrical double layer capacitor (EDLC). In contrast, pseudocapacitor materials (transition metal oxides and conducting polymers) can deliver much higher capacitance than graphene due to the fast Faradic redox reactions on the surface or near-surface of the electrode materials but poor stability [7]. Therefore, it is an effective way to improve the capacitor performance by the combination of graphene and pseudocapacitor materials in supercapacitor [8]. Among various pseudocapacitor materials, polyaniline (PANI) is considered as one of the best electrode materials for supercapacitor due to its low cost, easy synthesis, high conductivity and high specific capacitance (with a theoretical value of 2000 F g^{-1}) [9].

However, because of the aggregation of graphene with strong π-π interactions, the performance advantages of PANI/graphene composites cannot fully be displayed, which limits its further applications [10, 11]. Recently, three dimensional (3D) graphene foam (GF) has been attracted much attention. Various synthetic methods of 3D GF including the template and self-assembly methods have been developed in the past few years [12–17]. The porous structure of 3D GF not only possesses the excellent properties of graphene (high electrical conductivity, excellent mechanical properties and large specific surface areas) but also prevents the aggregation of graphene.

Some researches of PANI/GF composites have been reported in recent years. Meng et al. [18] prepared a PANI nanowire arrays (NWAs)/GF composite. CaCO$_3$ particles formed in graphene oxide (GO) aqueous dispersion were used as the template to fabricate GF and PANI NWAs were grown on the surface of GF by in-situ polymerization. Yu et al. [19]

✉ Hongyan Yue
  hyyue@163.com

1 School of Materials Science and Engineering, Harbin University of Science and Technology, Harbin 150040, People's Republic of China

2 Research Institute for Nuclear Problems Belarusian State University, Minsk, Belarus

fabricated a GF by a dipping method and reduction process. PANI NWAs were grown on the GF by in-situ polymerization. The symmetric device based on PANI/GF composite electrodes in the 1 M H_2SO_4 electrolyte exhibits an ultrahigh specific capacitance (790 F g^{-1}) owing to the well-ordered porous structure of the composite. Luo et al. [20] prepared PANI nanofibers/nitrogen-doped graphene hydrogels by a polymerization and hydrothermal process. It shows a high specific capacitance (610 F g^{-1} at 1 A g^{-1}) due to their 3D porous structures, formed conducting networks, high specific surface areas and fast electron/ion transfer. As described above, it is the most common way to obtain GF by preparation of GO followed by a reduction process, which is used to combine with PANI NWAs as supercapacitor electrode. However, the distorted structure and the incomplete reduction of graphene degrade the electrical conductivity, which decreases the electrochemical properties of the composite.

In order to further improve the electrochemical properties of the composite, Yu et al. [21] fabricated the GF by chemical vapor deposition (CVD) and PANI nanocones were vertically grown on the surface of GF by electrodeposition. This structure increases the specific surface area and provides the fast diffusion path for electrolyte ions. The material possesses a specific capacitance of 751.3 F g^{-1} in 1 M $HClO_4$ and has a high rate capability as well as good cycling stability. Pedrós et al. [22] developed a PANI nanofiber sponge (PANI-NFS)/GF composite by CVD and the controlled electrodeposition process. The PANI-NFS/GF composite combines the efficient electronic transport in the GF with the rapid diffusion of the electrolyte ions into the PANI-NFS with a large specific surface area. A high specific capacitance 1474 F g^{-1} is obtained at a current density of 0.47 A g^{-1} and the capacitance retention is 83% after 15,000 cycles.

In this paper, a 3D GF was prepared by CVD using nickel foam (NF) as the template. Then, the activation treatment of GF was carried out by concentrated nitric acid. Finally, PANI NWAs were grown on the surface of GF by in-situ polymerization to obtain PANI NWAs/GF composite. The integration between GF and PANI NWAs shows a synergistic effect, which leads to the enhanced performance of both electric double-layer capacitors and pesudocapacitors. The specific capacitance of PANI NWAs/GF can reach as high as 870 F g^{-1} at a current density of 1 A g^{-1}. Moreover, the electrode possesses an excellent cycle life with 80% capacitance retention after 1000 cycles at 6 A g^{-1}.

2 Experimental

2.1 Synthesis of GF

GF was prepared by CVD using NF as the template. The areal density and thickness of NF are ~0.042 g cm^{-2} and ~1.6 mm, respectively. NF was placed into the middle of tube furnace and heated to 1000 °C at a rate of 10 °C min^{-1} under Ar (500 sccm) and H_2 (200 sccm) atmosphere, the temperature was hold 20 min to clean the surface of NF. A CH_4 gas (20 sccm) was then introduced into the tube furnace at ambient pressure with the same amounts of Ar and H_2. After 10 min, CH_4 gas was turned off and the sample was rapidly cooled to room temperature at a rate of ~100 °C min^{-1}. The final sample (NF covered with graphene) was cut into 1×1 cm^2 pieces, a 4 wt% poly(methyl methacrylate) (PMMA, weight-averaged molecular mass Mw D996,000) ethanol solution was dropped on the surface of sample and then solidified at 200 °C for 1 h. A thin layer PMMA was used to prevent structural failure of the GF when the NF was etched away. The sample was then placed in an HCl (3 M) at 90 °C for overnight to completely remove the nickel. Finally, GF was obtained by dissolving the PMMA with hot acetone at 60 °C and heat-treated at 450 °C in Ar for 1 h.

2.2 Preparation of PANI NWAs/GF

Firstly, the GF was immersed in the concentrated nitric acid (16 M) for 18 h at room temperature and washed by deionized water for several times. The activated GF was transferred onto a glass slide and dried by freeze-drying. Then, the activated GF was carefully immersed into the solution of 1 M H_2SO_4 aqueous solution containing aniline (AR) for 3 h under ice bath to ensure the complete adsorption of aniline. The ammonium per oxydisulfate (APS, AR) was resolved in the same volume solution of 1 M H_2SO_4 aqueous solution. Finally, the APS solution was rapidly added to the aniline solution and stirred for 60 s, the molar ratio of aniline to APS was 4:1. Polymerization was carried out at −5 °C. After reacting for 24 h, the PANI NWAs/GF composite was taken out and washed with deionized water for several times. For comparison, the PANI/GF composite was also prepared using the same method without the activation process of GF.

2.3 Characterizations

The morphologies of the GF, PANI NWAs/GF were examined by field emission scanning electron microscopy (FE-SEM, FEI, Sirion-200) with an accelerating voltage of 20 kV. A high-resolution transmission electron microscope (HR-TEM; JEM2100F, JEOL) was used to investigate the morphologies of the GF. Raman spectroscopy was performed with a micro-Raman system (Renishaw, RM1000-In Via) in the range of 500–3000 cm^{-1} using an excitation energy of 1.96 eV (633 nm, HeNe laser).

2.4 Electrochemical measurements

The electrochemical studies were performed in a conventional three-electrode system with 1 M H_2SO_4 electrolyte solution. The PANI NWAs/GF was used as the working electrode, Ag/AgCl as the reference electrode and platinum wire as the counter electrode. The cyclic voltammetry (CV), electrochemical impedance spectroscopy (EIS) and galvanostatic charge/discharge (GCD) cycle tests were carried out on a Biologic VMP3 electrochemical workstation.

3 Results and discussion

Figure 1 shows the schematic of fabrication process of PANI NWAs/GF composite. Firstly, NF was used as the template

to deposit graphene on its surface by CVD. After etching of nickel, GF was obtained. Then, GF was activated by the concentrated nitric acid to obtain active groups on its surface. Finally, PANI NWAs were grown on the surface of the activated GF by in-situ polymerization.

SEM image of the free-standing GF is shown in Fig. 2a. An interconnected 3D network structure can be clearly observed. The graphene sheet has a smooth and complete surface, and the intrinsic grains and wrinkles of the graphene sheets well remained (Fig. 2b). The pore size of the GF is ~200 μm, which is similar to that of nickel foam. The pores are interconnected together, which ensures good electrical properties and high specific surface areas. The thickness of graphene sheets is ca. 3 nm (Fig. 2c), which is the typical thickness of few-layered graphene (<10 layers). A large-scale of dense and aligned PANI NWAs

Fig. 1 Schematic of fabrication process of the PANI NWAs/GF. **a** NF, **b** graphene/NF, **c** activated GF, **d** PANI NWAs/GF
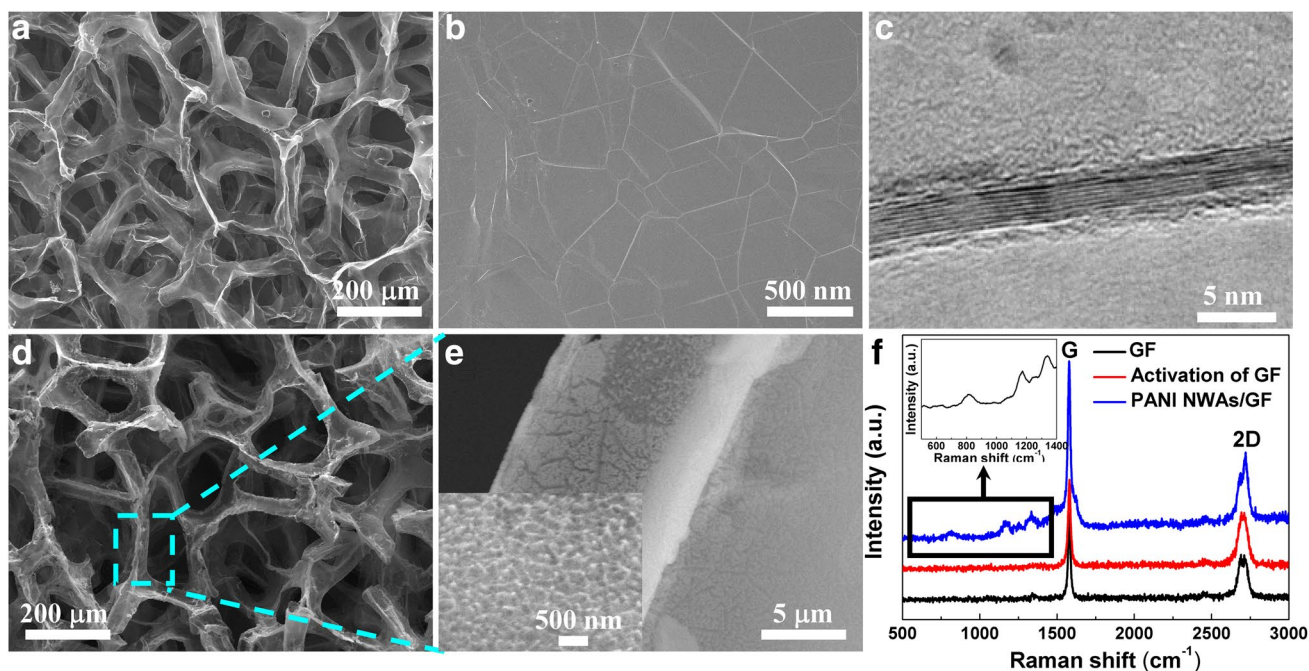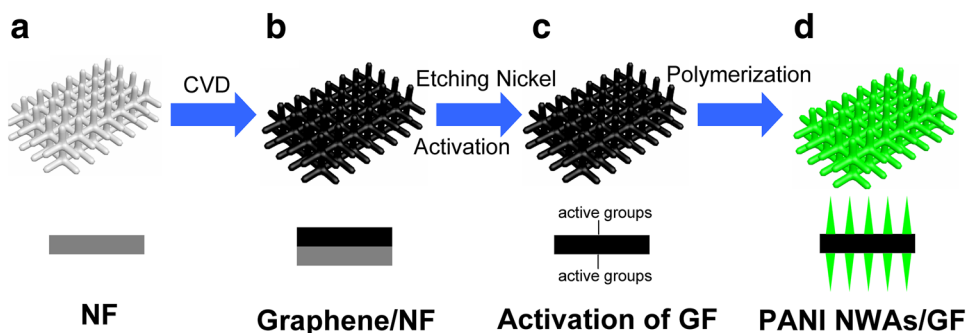
Fig. 2 Images and structure of the PANI NWAs/GF. **a** SEM image of GF after removal of nickel, **b** the surface morphology of GF without nickel, **c** HRTEM image of GF, **d** SEM image of PANI NWAs/GF, **e** magnified image of Fig. 2d (*inset* magnified image of PANI NWAs/GF), **f** Raman spectra of GF, activated GF and PANI NWAs/GF

are vertically and uniformly grown on the surface of GF (Fig. 2d, e). The Raman spectra of GF, activated GF and PANI NWAs/GF composite are shown in Fig. 2f. There are two prominent peaks at 1580 and 2712 cm^{-1} corresponding to the G band and 2D band of graphene. No appreciable D band is observed, which proves the high quality of graphene prepared by CVD [23]. The Raman spectrum of the activated GF does not change significantly, indicating that the excellent properties of graphene are not destroyed after activation treatment. Besides of the peaks of GF, the Raman spectrum of PANI NWAs/GF composite presents several representative peaks attributed to PANI: the C–N$^+$ stretching at 1340 cm^{-1}, the C–H bending of the benzenoid ring at 1251 cm^{-1}, the C–H bending of quinoid ring at 1171 cm^{-1}, the N–H bending of the benzenoid ring at 1070 cm^{-1}, C–H bending in the quinonoid ring at 810 cm^{-1} [20]. This also indicates that PANI NWAs are grown on the surface of GF. In addition, the morphologies of PANI NWAs/GF composite are highly affected by the polymerization time (Fig. 3). After polymerization for 8 h, short PANI NWAs with low density are grown on the surface of GF (Fig. 3a and b). After polymerization for 24 h, long PANI NWAs with high density forms on the surface of GF (Fig. 3 c and d). Meanwhile, it is also important to grow PANI NWAs on the surface of GF by activation treatment of GF. The morphologies of PANI/GF composite without the activation process of GF are shown in Fig. 4. As displayed in Fig. 4a, the surface of GF looks like smooth after polymerization process. Only some small protuberances can be observed on the surface of GF in enlarged views (Fig. 4b, c), which indicates that only a few PANI nuclei are produced. This is different from the activated GF, which has various oxygen functional groups on their surface, and these functional groups act as anchor sites and enable the subsequent in-situ polymerization of PANI attaching on the surface of GF. Moreover, the π-π stacking force between the phenyl and basal planes of GF is also beneficial to the in-situ polymerization on the surface of GF. Therefore, the PANI can gradually grow along the initial nuclei of PANI to form long PANI NWAs in a dilute solution and at a low temperature [10, 24].

The electrochemical properties of as-prepared PANI NWAs/GF composite are evaluated, as shown in Fig. 5. Figure 5a compares the CV curves of pristine GF and PANI NWAs/GF electrode collected at the scanning rate of 20 mV s^{-1}. The pristine GF exhibits a very low current density response. The CV loop area of PANI NWAs/GF composite is much larger than that of GF, which indicates that the electrochemical performance is significantly improved owing to anchoring the PANI NWAs on the surface of GF. Moreover, two pairs of redox peaks of A_1/C_1 and A_2/C_2 are found on the CV curves of PANI NWAs/GF composite. A_1/C_1 Peaks are attributed to the redox transitions of PANI between a semiconducting state (leucoemeraldine form) and a conducting state (polaronic emeraldine form). A_2/C_2 Peaks are attributed to the Faradaic transformation of emeraldine to pernigraniline (Fig. 6) [25–27]. CV curves of PANI NWAs/GF electrode at various scan rates of 10–100 mV s^{-1} are shown in Fig. 5b. With increasing the scan rate, the oxidation and

Fig. 3 SEM images of the PANI NWAs/GF obtained at different reaction time. **a** 8 h, **b** magnified image of Fig. 3a, c 24 h, **d** magnified image of Fig. 3c
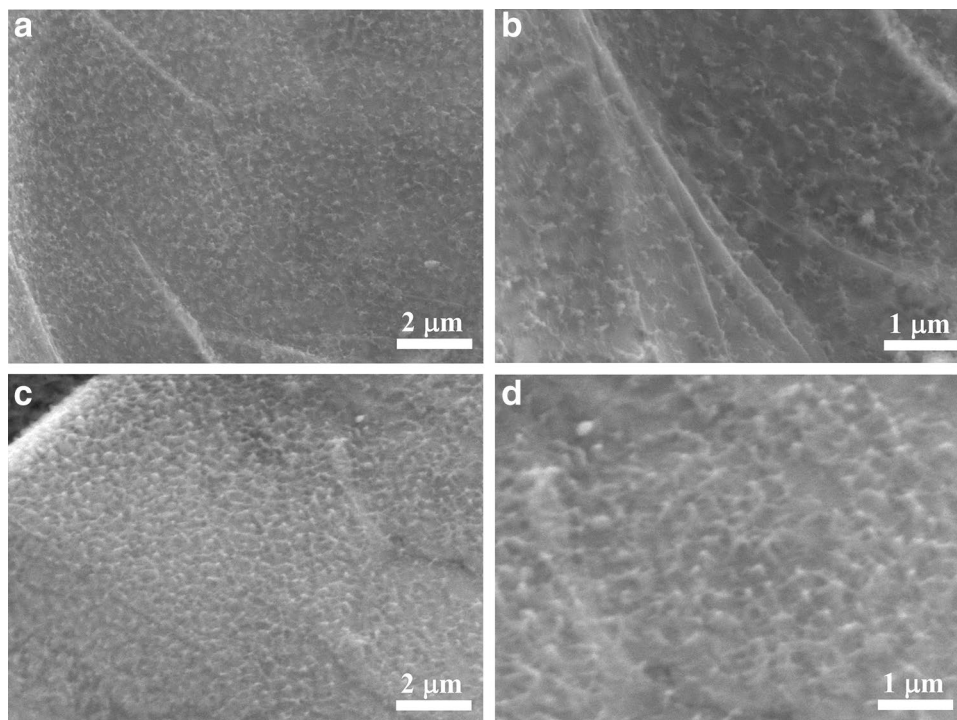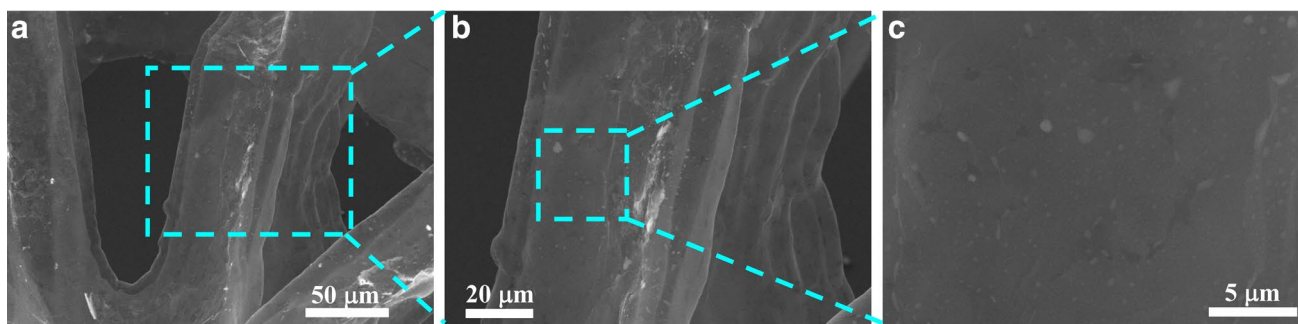
**Fig. 4** SEM images of the PANI/GF without the activation of GF at different magnifications
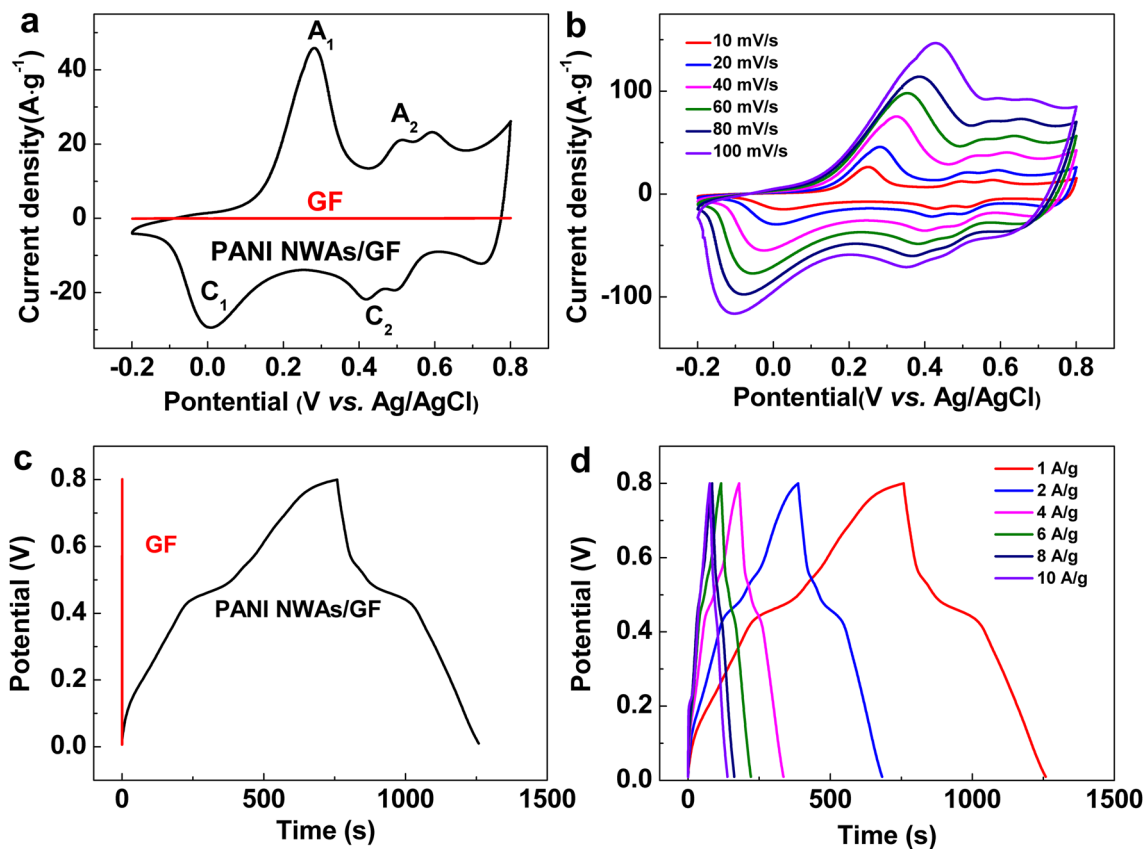
Fig. 5 Electrochemical performances of the PANI NWAs/GF. **a** CV curves of GF and PANI NWAs/GF within the potential window −0.2 to 0.8 V versus SCE at a scan rate of 20 mV s⁻¹, **b** CV curves of PANI NWAs/GF at various scan rates, **c** GCD curves of GF and PANI NWAs/GF at a current density of 1.0 A g⁻¹, **d** GCD curves of PANI NWAs/GF at various current densities

reduction peaks shift to the positive and negative positions, respectively. This is mainly owing to the resistance of PANI NWAs/GF electrode [3]. However, even at the high scan rate of 100 mV s⁻¹, the redox peaks of PANI are still well maintained, which indicates that PANI NWAs/GF electrode has a rapid charge–discharge response and a good rate performance. This can be explained by the shorter diffusion path of PANI NWAs for ion and the faster conductive channel of

GF. Figure 5c shows the GCD curves of the pristine GF and PANI NWAs/GF electrodes at the current density of 1 A g⁻¹. The longer charge–discharge time indicates that the PANI NWAs/GF electrode has a good capacitive behavior and the pseudocapacitive contribution comes from the PANI NWAs compared with the negligible charge/discharge time of pristine GF. Additionally, GCD measurements of PANI NWAs/ GF are carried out at various current densities ranging from
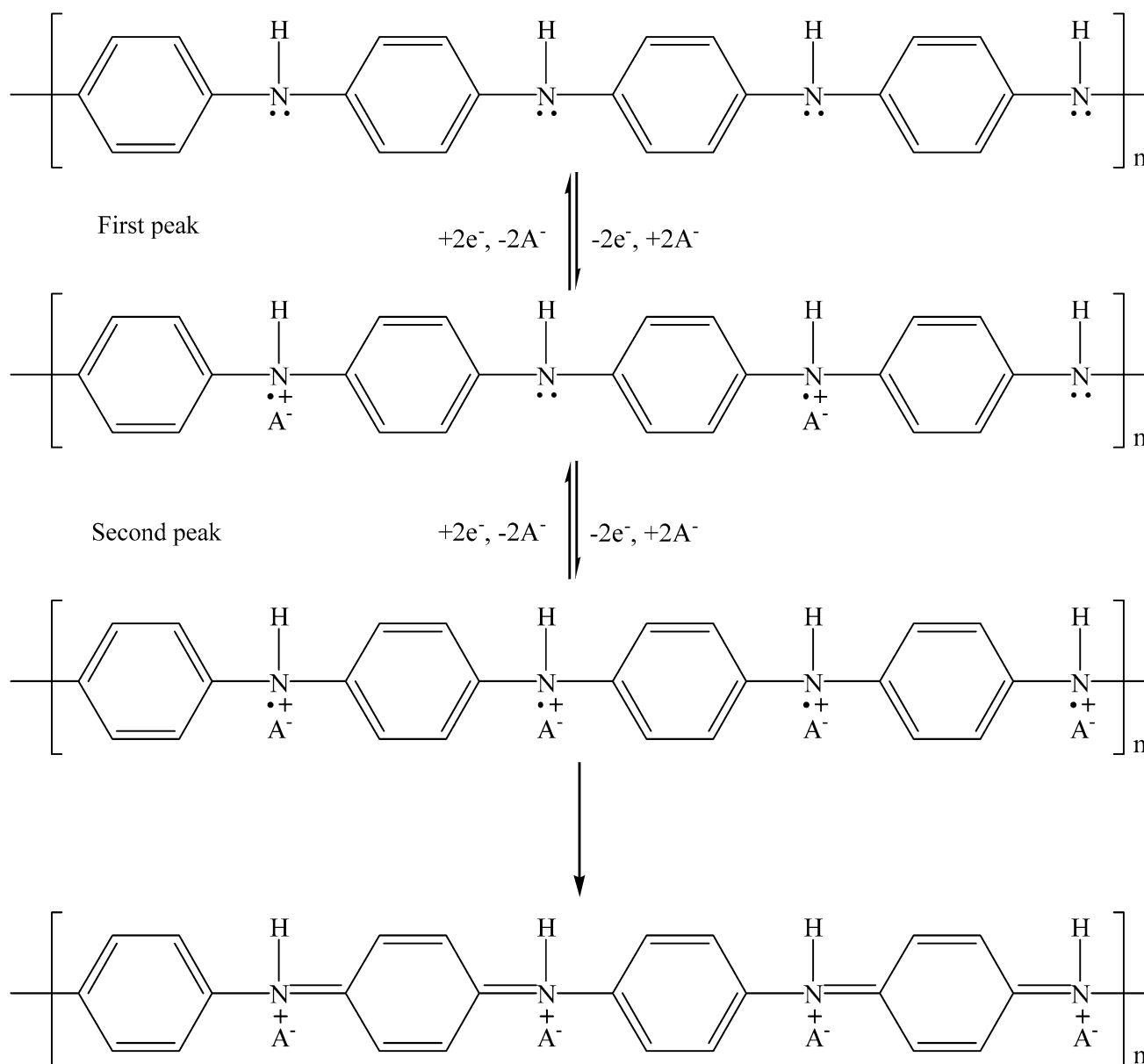
Fig. 6 Redox reactions of PANI

1 to 10 A g^{-1}, as shown in Fig. 5d. The symmetrical and linear charge–discharge curves at all current densities exhibit a high reversibility and a fast electronic response. For comparison, the CV and GCD curves of PANI/GF electrode with various scan rates and current densities are shown in Fig. 7. The weak oxidation peaks and fast discharging time indicate that the lack of PANI and poor electrochemical properties.

The specific capacitance values are calculated from the GCD curves according to the following equation: $C = I \times t / \Delta V \times m$, where C is specific capacitance (F g^{-1}), I and t are charge–discharge current and time, respectively, V is the change of charge–discharge voltage, which is 0.8 V in our measurement, and m is the mass of one piece of PANI

NWAs/GF electrode. The results of specific capacitance of the PANI NWAs/GF electrode are plotted in Fig. 8a. The specific capacitance of the electrode is 870 F g^{-1} at 1 A g^{-1}, which is much higher than that of PANI/GF electrode. When the current density increases, the specific capacitance of the electrode almost has a relative constant. The excellent capacitive performance of the PANI NWAs/GF electrode is attributed to the synergistic effect of GF with interconnected 3D network structure and PANI NWAs decorated on it. The highly conductive GF and the orderly structure of PANI NWAs provides a rapidly migration and diffusion path for electronic or ion during the charge/discharge process. As shown in Fig. 8b, Nyquist plot of the PANI NWAs/GF
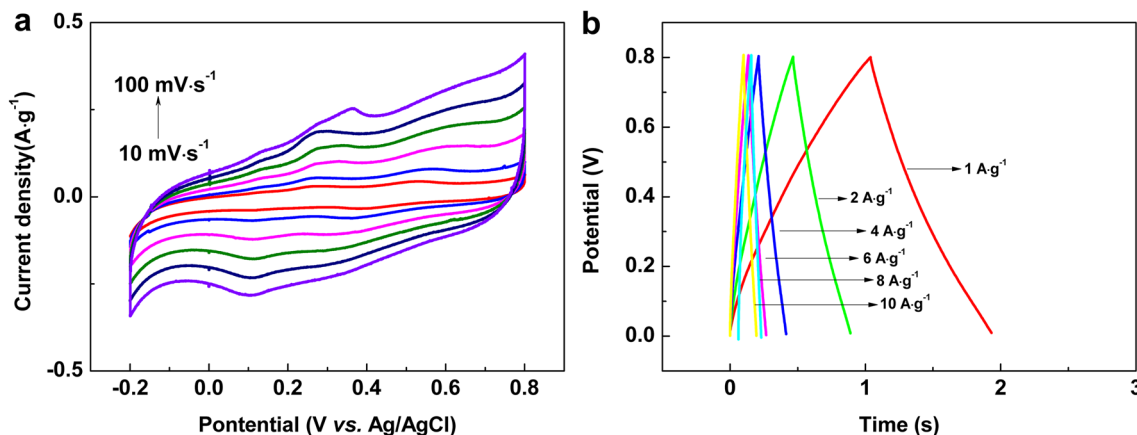
Fig. 7 Electrochemical performances of the PANI/GF without the activation of GF. **a** CV curves of PANI/GF at various scan rates, **b** GCD curves of PANI/GF at various current densities
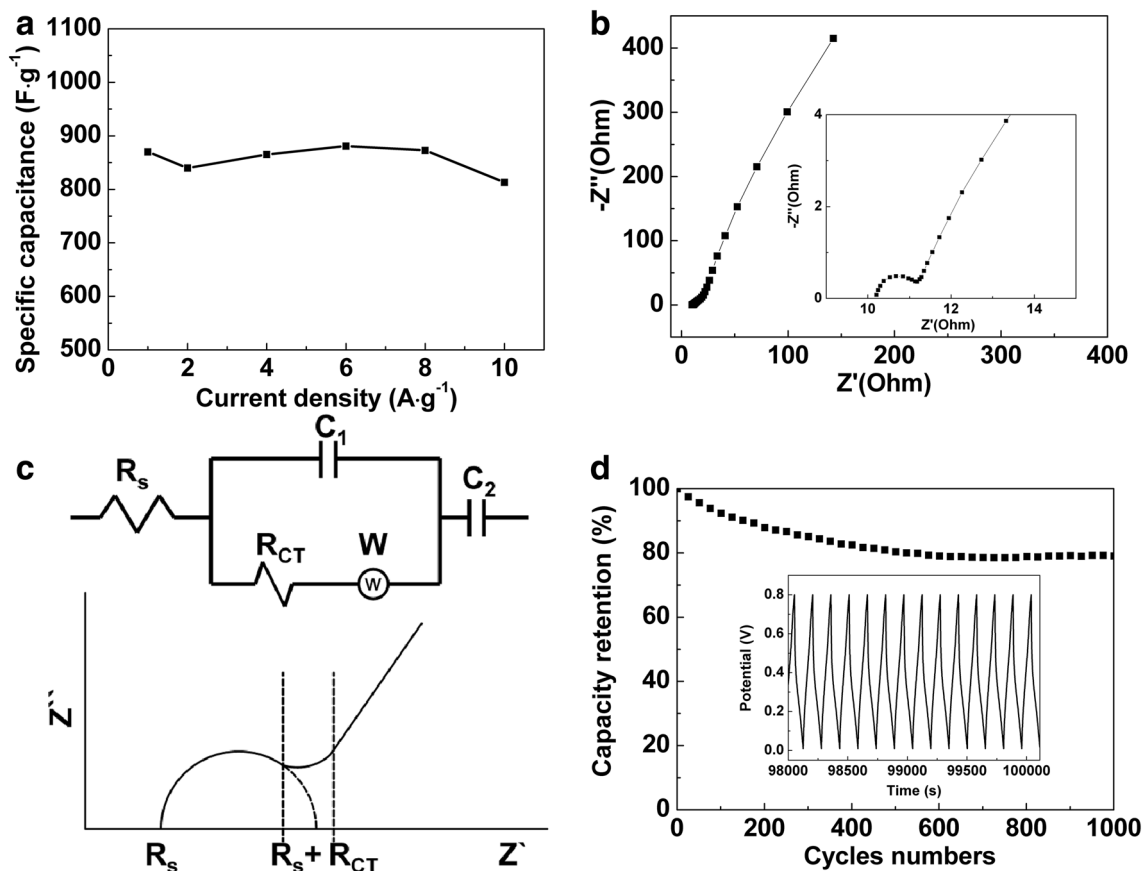
Fig. 8 Electrochemical performances of the PANI NWAs/GF. **a** Specific capacitance plots at current densities from 1 to 10 A g^{-1}, **b** Nyquist plots of supercapacitors based on PANI NWAs/GF (*inset* the high frequency region of Nyquist plots), **c** modeled equivalent circuit of electrochemical impedance spectroscopy, **d** cycle tests of the PANI NWAs/GF with a GCD current density of 6 A g^{-1}

electrode is obtained in the frequency range from 10 mHz to 100 kHz at open circuit potential with an ac perturbation of 5 mV and an expanded view of the high-frequency region is shown in the inset of Fig. 8b. The Nyquist plot obtained is modeled and interpreted with the help of an appropriate electric equivalent circuit (Fig. 8c), where R$_s$ stands for a

equivalent series resistances (active material/current collector contact resistance, electrolyte resistance), which can be suggested by the x intercept of the Nyquist plot, R_{ct} is the charge transfer resistance at the electrode/solution interface, which can be suggested by the semi-circle in the high frequency, the Warburg type element related to electrolyte ions diffusion, C_1 is the double layer capacitance and C_2 is the Faradic capacitance [28]. As shown in Fig. 8b, the PANI NWAs/GF electrode exhibits a high R_s value (10 Ω), this is mainly attributed to the high resistance of current collector. The small semicircle diameter indicates that PANI NWAs/GF has a small R_{ct}, which results in a good electrochemical performance. Moreover, a small Warburg resistance can be observed from Nyquist plot, which proves a good charge transfer behavior of PANI NWAs/GF electrode. As displayed in Fig. 8d, the cycle life of the PANI NWAs/GF electrode is conducted at 6 A g^{-1}. After 1000 cycles, the specific capacitance of PANI NWAs/GF electrode retains 80%. The close bonding between the GF and PANI NWAs effectively improves the long-term stability. Moreover, the GF as a support skeleton allows the uniform deposition of PANI NWAs on its surface, which provides an effective strain relaxation for PANI NWAs. The decreased specific capacitance of PANI NWAs/GF electrode can be attributed to the failure and overoxidation of the PANI NWAs, leading to the deterioration of polymeric conductivity and charge storage capability during the charge/discharge process.

All the results prove that the PANI NWAs/GF composite has a good capacitance properties and excellent cycling stability. It can be attributed to the following reasons: firstly, the high conductivity and interconnected 3D network structure of GF fabricated by CVD could serve as a rapid transfer path for electronic. Secondly, the well-organized PANI NWAs uniformly anchored on the surface of GF exhibit a large specific surface area and a short ion diffusion path, which provides a high specific capacitance. Thirdly, the synergistic effect between GF and PANI NWAs makes the full utilization of composite, causing both high specific capacitance and cyclic stability. However, the strength of the PANI NWAs/GF composite has not reached the expected, thus the stability of the PANI NWAs/GF composite needs to be further improved.

4 Conclusions

In summary, GF is prepared by CVD using nickel foam as the template. After activation treatment of GF by concentrated nitric acid, PANI NWAs are grown on the surface of GF by in-situ polymerization to obtain PANI NWAs/GF. Owing to the synergistic effect of GF and PANI NWAs, the PANI NWAs/GF exhibits a high specific capacitance (870 F g^{-1} at 1 A g^{-1}) and 80% capacitance retention after 1000 cycles at 6 A g^{-1}.

References

1. P. Simon, Y. Gogotsi, Materials for electrochemical capacitors. Nat. Mater. **7**, 845–854 (2008)
2. L.F. Chen, Z.Y. Yu, X. Ma, Z.Y. Li, S.H. Yu, In situ hydrothermal growth of ferric oxides on carbon cloth for low-cost and scalable high-energy-density supercapacitors. Nano Energy **9**, 345–354 (2014)
3. V. Senthilkumar, F.B. Kadumudi, N.T. Ho, J.W. Kim, S. Park, J.S. Bae, W.M. Choi, S. Cho, Y.S. Kim, NiO nanoarrays of a few atoms thickness on 3D nickel network for enhanced pseudocapacitive electrode applications. J. Power Sources **303**, 363–371 (2016)
4. K.S. Novoselov, A.K. Geim, S.V. Morozov, D. Jiang, Y. Zhang, S.V. Dubonos, I.V. Grigorieva, A.A. Firsov, Electric field in atomically thin carbon films. Science **306**, 666–669 (2004)
5. C. Liu, Z. Yu, D. Neff, A. Zhamu, B.Z. Jang, Graphene-based supercapacitor with an ultrahigh energy density. Nano Lett. **10**, 4863–4868 (2010)
6. A. Yu, I. Roes, A. Davies, Z. Chen, Ultrathin, transparent, and flexible graphene films for supercapacitor application. Appl. Phys. Lett. **96**, 253105 (2010)
7. M. Beidaghi, Y. Gogotsi, Capacitive energy storage in micro-scale devices: recent advances in design and fabrication of micro-supercapacitors. Energy Environ. Sci. **7**, 867–884 (2014)
8. Z.S. Wu, G. Zhou, L.C. Yin, W. Ren, F. Li, H.M. Cheng, Graphene/metal oxide composite electrode materials for energy storage. Nano Energy **1**, 107–131 (2012)
9. K.N. Ashok, J.B. Baek, Electrochemical supercapacitors from conducting polyaniline-graphene platforms. Chem. Commun. **50**, 6298–6308 (2014)
10. J.J. Xu, K. Wang, S.Z. Zu, B.H. Han, Z. Wei, Hierarchical nanocomposites of polyaniline nanowire arrays on graphene oxide sheets with synergistic effect for energy storage. ACS Nano **4**, 5019–5026 (2010)
11. Q. Wu, Y.X. Xu, Z.Y. Yao, A.R. Liu, G.Q. Shi, Supercapacitors based on flexible graphene/polyaniline nanofiber composite films. ACS Nano **4**, 1963–1970 (2010)
12. B.G. Choi, M.H. Yang, W.H. Hong, J.W. Choi, Y.S. Huh, 3D macroporous graphene frameworks for supercapacitors with high energy and power densities. ACS Nano **6**, 4020–4028 (2012)
13. J. Sha, C. Gao, S.K. Lee, Y. Li, N. Zhao, J.M. Tour, Preparation of three-dimensional graphene foams using powder metallurgy templates. ACS Nano **10**, 1411–1416 (2016)
14. Y. Xu, K. Sheng, C. Li, G. Shi, Self-assembled graphene hydrogel via a one-step hydrothermal process. ACS Nano **4**, 4324–4330 (2010)
15. Z. Niu, J. Chen J.H.H. Huey, J. Ma, X. Chen, A leavening strategy to prepare reduced graphene oxide foams. Adv. Mater. **24**, 4144–4150 (2012)
16. H. Sun, Z. Xu, C. Gao, Multifunctional, ultra-flyweight, synergistically assembled carbon aerogels. Adv. Mater. **25**, 2554–2560 (2013)

17. Z. Chen, W. Ren, L. Gao, B. Liu, S. Pei, H.M. Cheng, Three-dimensional flexible and conductive interconnected graphene networks grown by chemical vapour deposition. Nat. Mater. **10**, 424–428 (2011)
18. Y. Meng, K. Wang, Y. Zhang, Z. Wei, Hierarchical porous graphene/polyaniline composite film with superior rate performance for flexible supercapacitors. Adv. Mater. **25**, 6985–6990 (2013)
19. P.P. Yu, X. Zhao, Z.L. Huang, Y.Z. Li, Q.H. Zhang, Free-standing three-dimensional graphene and polyaniline nanowire arrays hybrid foams for high-performance flexible and lightweight. J. Mater. Chem. A **2**, 14413–14420 (2014)
20. J. Luo, W. Zhong, Y. Zou, C. Xiong, W. Yang, Preparation of morphology-controllable polyaniline and polyaniline/graphene hydrogels for high performance binder-free supercapacitor electrodes. J. Power Sources **319**, 73–81 (2016)
21. M. Yu, Y.X. Ma, J.H. Liu, S.M. Li, Polyaniline nanocone arrays synthesized on three-dimensional graphene network by electrodeposition for supercapacitor electrodes. Carbon **87**, 98–105 (2015)
22. J. Pedrós, A. Boscá, J. Martínez, S. Ruiz-Gómez, L. Pérez, V. Barranco, F. Calle, Polyaniline nanofiber sponge filled graphene foam as high gravimetric and volumetric capacitance electrode. J. Power Sources **317**, 35–42 (2016)
23. A.C. Ferrari, J.C. Meyer, V. Scardaci, C. Casiraghi, M. Lazzeri, F. Mauri, S. Piscanec, D. Jiang, K.S. Novoselov, S. Roth, A.K. Geim, Raman spectrum of graphene and graphene layers. Phys. Rev. Lett. **97**, 187401 (2006)
24. P. Yu, Y. Li, X. Zhao, L. Wu, Q. Zhang, Graphene-wrapped polyaniline nanowire arrays on nitrogen-doped carbon fabric as novel flexible hybrid electrode materials for high-performance supercapacitor. Langmuir **30**, 5306–5313 (2014)
25. N.A. Kumar, H.J. Choi, Y.R. Shin, D.W. Chang, L. Dai, J.B. Baek, Polyaniline-grafted reduced graphene oxide for efficient electrochemical supercapacitors. ACS Nano **6**, 1715–1723 (2012)
26. H. Li, J. Wang, Q. Chu, Z. Wang, F. Zhang, S. Wang, Theoretical and experimental specific capacitance of polyaniline in sulfuric acid. J. Power Sources **190**, 578–586 (2009)
27. F. Fusalba, P. Gouérec, D. Villers, D. Bélanger, Electrochemical characterization of polyaniline in nonaqueous electrolyte and its evaluation as electrode material for electrochemical supercapacitors. J. Electrochem. Soc. **148** A1–A6 (2001)
28. J. Chang, M. Jin, F. Yao, T.H. Kim, V.T. Le, H. Yue, F. Gunes, B. Li B.A. Ghosh, S. Xie, Y.H. Lee, Asymmetric supercapacitors based on graphene/MnO_2 nanospheres and graphene/MoO_3 nanosheets with high energy density. Adv. Funct. Mater. **23**, 5074–5083 (2013)